Devagiri Journal of Science 2(1), 65-78

www.devagirijournals.com
ISSN 2454-2091

Growth and spectral characterization of nonlinear optical crystal L-Asparaginium tartrate

Sreelaja P.V. and Ravikumar C. *

Nanotechnology and Advanced Materials Research Centre, Department of Physics, CMS College, Kottayam, Kerala, India.

Received: 19. 07.2016
Revised and Accepted: 21.08.2016

Key Words: *Ab initio*; DFT; FT-IR; FT-Raman

Abstract: The Fourier Transform Raman spectra in the region 3500–50 cm^{-1} and the Infra-red spectra in the range 4000-400 cm^{-1} of the crystallized NLO crystal L-Asparaginium tartrate (LAT) have been recorded. The geometry, intermolecular hydrogen bond, and harmonic vibrational frequencies of LAT have been investigated with the help of B3LYP density functional theory (DFT) methods. The calculated molecular geometry has been compared with the experimental data obtained from XRD data. The redshifting of both O-H and NH_3^+ stretching wavenumber confirms the intra- and intermolecular O-H···O and N- H···O hydrogen bonding respectively. The blueshifting of NH_2 stretching wavenumbers indicates the formation of intramolecular N-H···O hydrogen bonding. The optimized geometry shows, the carbon skeleton of the tartrate molecule is non-planar. The lowering of HOMO and LUMO energy gap supports the NLO activity of the molecule.

Introduction

In recent years, there is a growing need for nonlinear optical (NLO) materials in view of their applications in opto-electronic and photonic devices (Chemla & Zyss, 1987). In terms of nonlinear optical properties, organic compounds possess more advantages as compared to their inorganic counterparts (Hierle *et al*., 1984; Dicoll *et al*., 1986). In the solid state, amino acids exhibit a zwitterionic behavior in that they contain a protonated amino group (NH_3^+) and deprotonated carboxylic acid group (COO^-). This dipolar nature leads to some interesting physical and chemical properties in amino acids making them suitable candidates for NLO applications (Mallik *et al*., 2006). Also one of the advantages in working with organic materials is that they allow one to fine-tune the chemical structures and properties for the desired nonlinear optical properties (Datta & Pati, 2003). In addition, they have large structural diversity. The properties of organic compounds can be refined using molecular engineering and chemical synthesis (DeMatos *et al*., 2000). Hence they are projected as forefront candidates for fundamental and applied investigations.

The design of organic polar crystals for quadratic NLO applications is supported by the observation that organic molecules containing ð electron systems asymmetrized by electron donor and acceptor groups are highly polarisable entities (Pecaut & Bagieu-Beucher, 1993). The naturally occurring amino acid L-asparagine plays a role in the metabolic control of some cell functions in nerveand brain tissues and is also used by many plants as a nitrogen reserve source (Casado *et al*., 1995). Recently, the growth and characterization of the single crystals of the NLO materials, viz., L- asparaginium picrate (Srinivasan *et al*., 2006) and Lasparagine monohydrate Shakir *et al*., (2010) have been reported. Vibrational spectroscopy is a proficient tool for characterization of crystalline materials. It is effectively used to identify functional groups and determining

*Corresponding author
E-mail: rkr.ravi@gmail.com

the molecular structure of synthesized crystals. Theoretical simulations can certainly assist to obtain a deeper understanding of the vibrational spectra of complicated molecules. Recently it was shown that density functional theory (DFT) methods are a powerful computational alternative to the conventional quantum chemical methods, since they are much less computationally demanding and take account of the effects of electron correlation (Ravikumar *et al*., 2008; Ravikumar *et al*., 2010 and Ravikumar & Joe, 2010) . The present work deals with growth and detailed vibrational spectral investigation of the crystal L-Asparaginium tartrate elucidate the correlation between the molecular structure and NLO activity, charge transfer interactions and hydrogen bonding of the molecule aided by using density functional theory (DFT) computation.

Experimental

Synthesis

Single crystals of L-Asparaginium tartrate (LAT) were grown by slow evaporation technique dissolving L-Asparagine (99% Aldrich) with the aqueous solution of tartratic acid (99% Aldrich) in the 1:1 stoichiometric ratio. Colourless, transparent crystals of LAT were obtained within few weeks. The LAT crystals were subjected to repeated recrystallization to get good quality crystals.

Spectroscopic measurements

The FT-IR spectrum of BTSC was recorded using Perkin Elmer RXI spectrometer in the region 4000-400 cm^{-1}, with samples in the KBr. The resolution of the spectrum is 4 cm^{-1}.

The NIR-FT Raman spectrum was obtained in the range 3500 – 50 cm^{-1} using Bruker RFS 27 FT Raman spectrophotometer with a 1064 nm Nd: YAG laser source of 100 mW power. Liquid nitrogen cooled Ge-diode was used as a detector. Spectra were collected for samples with 1000 scan accumulated for over 30 minute's duration. The spectral resolution after apodization was 2 cm^{-1}.

Computational Details

The quantum chemical computations of LAT has been performed using Gaussian '09 program package (Kong *et al*., 2008) at the Becke3-Lee-Yang-Parr (B3LYP) level with standard6-31G* basis set. The optimized geometry corresponding to the minimum on the potential energy surface has been obtained by solving self-consistent field equation iteratively. The harmonic vibrational wave numbers have been analytically calculated by taking the second order derivative of energy using the similar level of theory. An empirical scaling factor of 0.8953 has been used to offset the systematic error caused by neglecting of an harmonicity and electron correlation (Frisch *et al*., 2009).Raman activities (S_i) calculated by Gaussian '09 program have been converted to relative Raman intensities (I_i) using the following relationship derived from the basic theory of Raman scattering (Scott & Radom, 1996).

$$I_i = \frac{f(\nu_o - \nu_i)^4 S_i}{\nu_i \left[1 - \exp\left(\frac{-hc\nu_i}{kT}\right)\right]} \qquad (1)$$

Where ν_o is the exciting wavenumber, $\nu_i$is the vibrational wavenumber of the i^{th} normal mode, h and k are universal constants and 'f' is the suitably chosen common scaling factor for all the peak intensities. The simulated IR and Raman spectra have been plotted using pure Lorentzian band shapes with full width half maximum of 10 cm^{-1}.

Results and Discussion

Optimized Geometry

The optimized molecular structure of the isolated LAT molecule calculated using DFT theory at B3LYP/6-31* level is shown in Fig. 1. The optimized geometrical parameters are

given in Table 1 with the comparison of experimental values (Natarajan*et al.*, 2010). The calculated bond length of C_{20}-O_{19} and C_{20}-O_{21} of the carboxyl group is 1.230 and 1.244 Å. This difference in bond length between C=O of the tartarate moiety is due to different environment of oxygen. The carbon skeleton of the tartrate molecule is non-planar, with a C_{20}-C_{22}-C_{26}-C_{30} torsion angle of - 175.68°. The $H_{17}\cdots O_{19}$ distance 1.819 Å is significantly shorter than the van der Waals separation between the O atom and the H atom demonstrating the possibility of N-H···O hydrogen bonding.

Table 1. Optimized parameters (Å, °) of LAT by B3LYP/6-31G* basis set

Bond length			*Bond angle*			*Dihedral angle*		
Parameter	*Cal.*	*[a]Exp.*	*Parameters*	*Cal.*	*[a]Exp.*	*Parameter*	*Cal.*	*[a]Exp.*
N_1-C_2	1.355	1.311	C_3-C_2-N_1	117.13	118.69	C_4-C_3-C_2-N_1	95.93	95.86
C_3-C_2	1.511	1.508	C_4-C_3-C_2	111.09	110.01	H_5-N_1-C_2-C_3	-158.49	176.45
C_4-C_3	1.541	1.533	H_5-N_1-C_2	115.64	119.98	H_6-N_1-C_2-C_3	-16.8	3.57
H_5-N_1	1.0	0.86	H_6-N_1-C_2	117.98	120.02	O_7-C_2-C_3-C_4	-82.16	-80.68
H_6-N_1	0.996	0.86	O_7-C_2-C_3	120.89	118.53	H_8-C_3-C_2-N_1	-144.87	143.41
O_7-C_2	1.209	1.247	H_8-C_3-C_2	108.45	109.68	H_9-C_3-C_2-N_1	-24.89	-24.77
H_8-C_3	1.083	0.97	H_9-C_3-C_2	112.21	109.67	H_{10}-C_4-C_3-C_2	-62.51	-53.97
H_9-C_3	1.081	0.97	H_{10}-C_4-C_3	110.45	107.84	C_{11}-C_4-C_3-C_2	169.49	-173.92
H_{10}-C_4	1.079	0.98	C_{11}-C_4-C_3	112.65	114.45	O_{12}-C_{11}-C_4-C_3	-79.67	36.45
C_{11}-C_4	1.542	1.533	O_{12}-C_{11}-C_4	114.38	35.24	O_{13}-C_{11}-C_4-C_3	52.98	148.98
O_{12}-C_{11}	1.28	1.271	O_{13}-C_{11}-C_4	108.55	117.54	H_{14}-O_{13}-C_{11}-C_4	-143.18	-175.9
O_{13}-C_{11}	1.411	1.22	H_{14}-O_{13}-C_{11}	103.51	109.45	N_{15}-C_4-C_3-C_2	55.2	63.94
H_{14}-O_{13}	0.948	0.82	N_{15}-C_4-C_3	109.2	111.09	H_{16}-N_{15}-C_4-C_3	105.98	-86.57
N_{15}-C_4	1.5	1.493	H_{16}-N_{15}-C_4	103.13	109.47	H_{17}-N_{15}-C_4-C_3	-130.5	-92.56
H_{16}-N_{15}	1.022	0.89	H_{17}-N_{15}-C_4	112.53	109.48	H_{18}-N_{15}-C_4-C_{11}	-131.94	27.45
H_{17}-N_{15}	1.024	0.89	H_{18}-N_{15}-C_4	111.88	109.49	O_{19}-H_{17}-N_{15}-C_4	96.43	-73.05
H_{18}-N_{15}	1.009	0.89	C_{20}-$O_{19}\cdots H_{17}$	114.89	109.47	C_{20}-O_{19}-H_{17}-N_{15}	-76.09	-132.82
C_{20}-O_{19}	1.23	1.306	O_{21}-C_{20}-O_{19}	128.68	125.76	O_{21}-C_{20}-O_{19}-H_{17}	-17.65	3.68
O_{21}-C_{20}	1.244	1.205	C_{22}-C_{20}-O_{19}	117.84	112.11	C_{22}-C_{20}-O_{19}-H_{17}	158.19	-177.83
C_{22}-C_{20}	1.539	1.522	H_{23}-C_{22}-C_{20}	110.6	108.7	H_{23}-C_{22}-C_{20}-O_{21}	-159.3	-130.74
H_{23}-C_{22}	1.079	0.98	O_{24}-C_{22}-C_{20}	110.48	110.6	O_{24}-C_{22}-C_{20}-O_{19}	144.88	169.94

O_{24}-C_{22}	1.4	1.422	H_{25}-O_{24}-C_{22}	105.88	109.5	H_{25}-O_{24}-C_{22}-C_{20}	24.05	40.49
H_{25}-O_{24}	0.952	0.82	C_{26}-C_{22}-C_{20}	107.56	108.52	C_{26}-C_{22}-C_{20}-O_{19}	-95.15	-67.32
C_{26}-C_{22}	1.544	1.532	H_{27}-C_{26}-C_{22}	108.13	109.82	H_{27}-C_{26}-C_{22}-C_{20}	67.7	71.2
H_{27}-C_{26}	1.088	0.98	O_{28}-C_{26}-C_{22}	112.21	112.14	O_{28}-C_{26}-C_{22}-C_{20}	-54.07	-51.23
O_{28}-C_{26}	1.393	1.41	H_{29}-O_{28}-C_{26}	107.91	109.5	H_{29}-O_{28}-C_{26}-H_{27}	-107.05	-50.76
H_{29}-O_{28}	0.955	0.82	C_{30}-C_{26}-C_{22}	110.15	108.81	C_{30}-C_{26}-C_{22}-C_{20}	-175.68	-168.48
C_{30}-C_{26}	1.517	1.528	O_{31}-C_{30}-C_{26}	127.5	122.03	O_{31}-C_{30}-C_{26}-C_{22}	118.28	120.25
O_{31}-C_{30}	1.184	1.216	O_{32}-C_{30}-C_{26}	110.77	113.6	O_{32}-C_{30}-C_{26}-C_{22}	-63.27	-60.59
O_{32}-C_{30}	1.339	1.302	H_{33}-O_{32}-C_{30}	107.25	109.47	H_{33}-O_{32}-C_{30}-C_{26}	178.64	-175.9
H_{33}-O_{32}	0.951	0.						
O_{19}···H_{17}	1.819	2.						

[a]Taken from Natarajan *e*

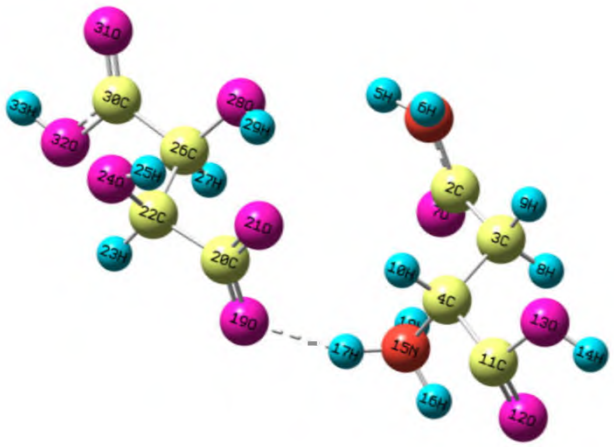

Fig. 1. Optimized molecular structure of LAT calculated at B3LYP/6-31G*

Vibrational Spectral Analysis

The vibrational spectral analysis is performed on the basis of the characteristic vibrations of the asparaginiumcation and tartrate anion. The detailed vibrational assignments of fundamental modes along with the calculated IR and Raman intensities and normal mode description are shown in Table 2. For visual comparison, the observed and simulated FTIR and FT-Raman spectra are presented in Figs. 2 and 3 respectively. Atomic displacements corresponding to selected normal modes of LAT are shown in Fig. 4.

NH_2 vibrations

The NH_2 stretching vibrations occur near 3380 and 3180 cm^{-1} for asymmetric and symmetric stretching vibrations (Vein *et al.,* 1991). The asymmetric NH_2 stretching is observed as a strong band in IR at 3351 cm^{-1}. The band at 3322 cm^{-1} in IR is assigned to symmetrical NH_2 stretching mode.

The blueshifting of NH_2 symmetric stretching wavenumber is due to the formation of intramolecular N-H···O hydrogen bonding. The NH_2 scissoring appears as strong band in IR at 1581 cm^{-1} and a medium band in Raman at 1591 cm^{-1}. The NH_2 out-of-plane vibrations are shown in Table 2.

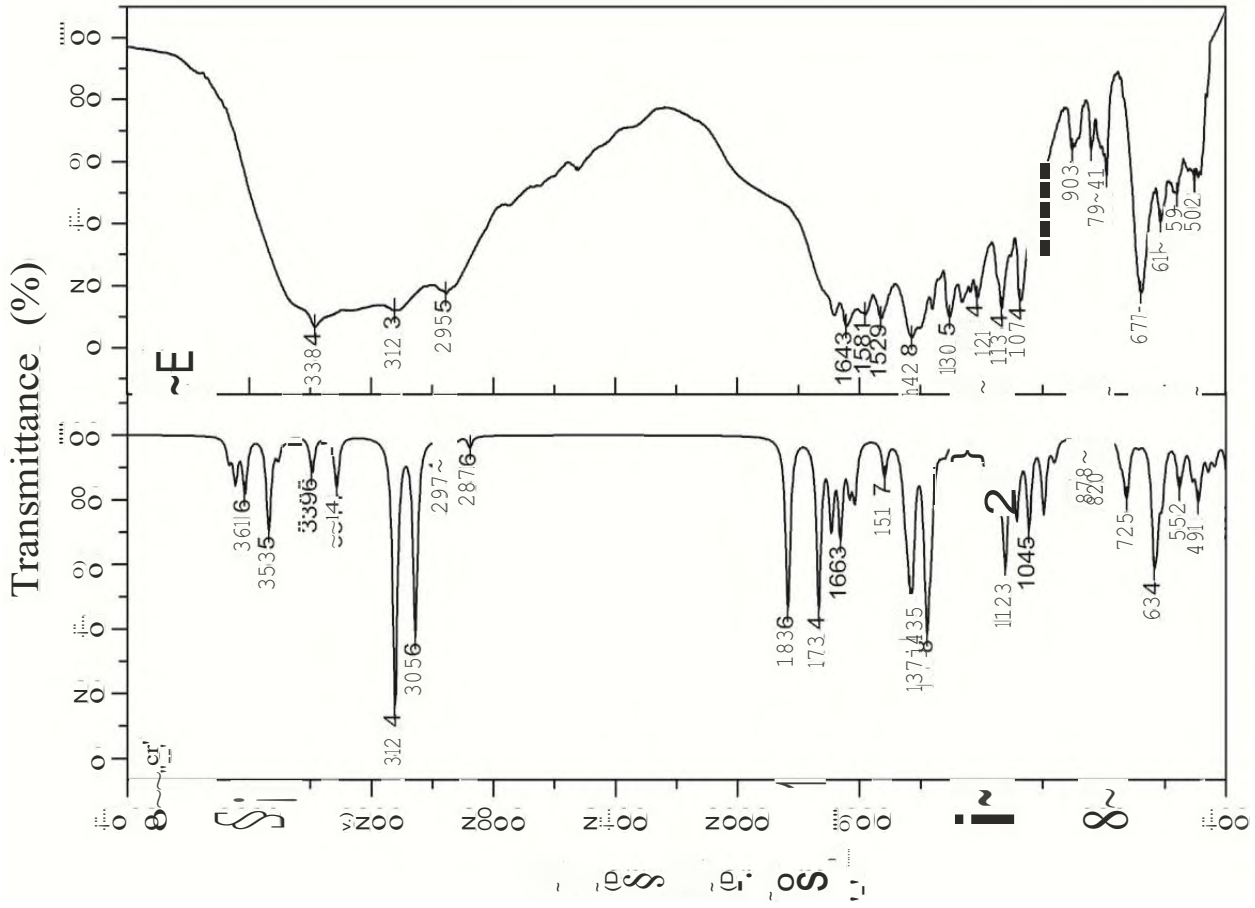

Fig. 2.(a) The FT-IR spectrum of LAT molecule in the wavenumber range 4000-400 cm^{-1}. **(b).** The simulated IR spectra of LAT molecule computed at B3LYP/6-31G* basis set

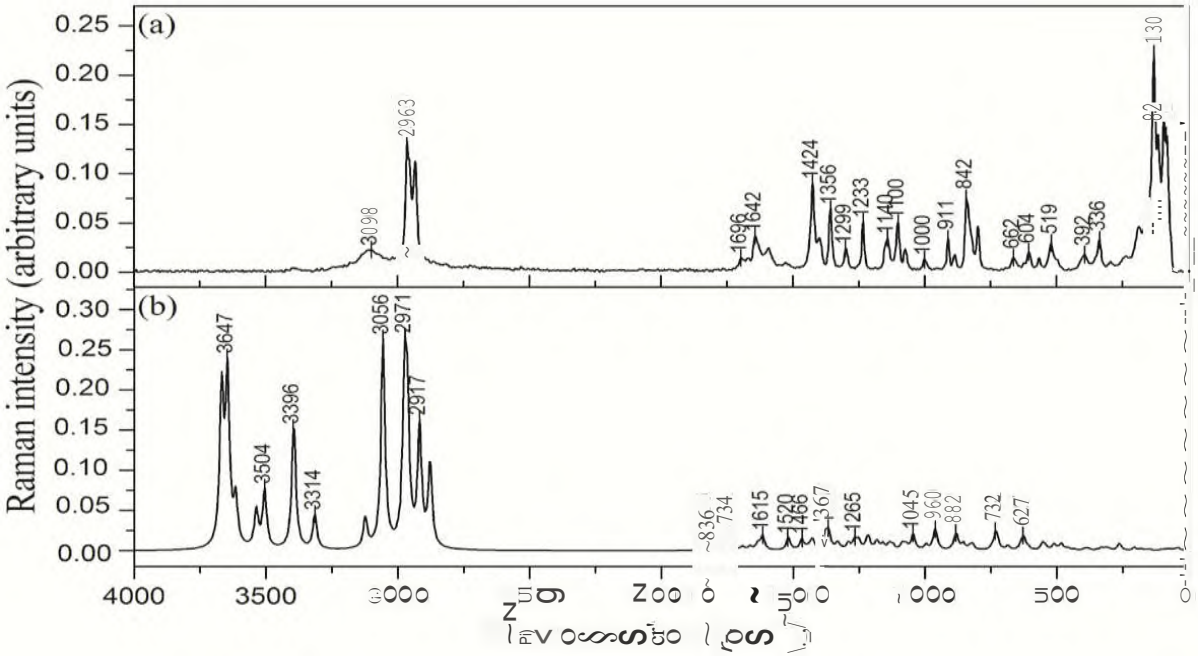

Fig. 3. (a). The FT-Raman spectrum of LAT in the wavenumber range 3500 –50 cm^{-1}.**(b).** The simulated Raman spectra of LAT molecule computed at B3LYP/6-31G* basis set

NH_3^+ group vibration

The NH_3^+ group vibrations usually appear in the region 3330 cm^{-1} for asymmetric stretching and 3080 cm^{-1} for symmetric stretching (Bellamy, 1975). The strong band observed in IR at 3123 cm^{-1} corresponds to NH_3 asymmetric stretching mode. The NH_3 symmetric stretching vibrations are observed as a medium band in Raman at 3098 cm^{-1}. The redshifting of NH_3^+ asymmetric stretching wavenumber indicate the formation of intermolecular N-H···O hydrogen bonding. The NH_3 asymmetric deformation vibrations normally appear in the region 1660-1610 cm^{-1}(Silverstein & Webster, 2003). In LAT, NH_3 asymmetric deformation vibration is coupled with COO^- asymmetric stretching mode and observed as strong bands at 1643 and 1642 cm^{-1} in IR and Raman respectively.

Table 2. Vibrational assignment of LAT along with IR and Raman intensities

ν_{cal}	IR intensity	Raman intensity	ν_{IR}	ν_{Raman}	Assignments
3668	50.08	94.76	3439 s	-	O_{13}-H_{14} stretch
3647	98.5	103.96	-	-	O_{32}-H_{33} stretch
3616	127.42	28.68	-	-	O_{24}-H_{25} stretch
3535	219.18	23.19	3384 br	3392 w	O_{28}-H_{29} stretch
3504	42.24	35.96	3351 s	-	NH_2asym. stretch
3396	85.52	77.38	3322 sh	-	NH_2 sym. stretch
3314	118.59	21.1	-	-	NH_3 asym. stretch
3124	631.44	18.28	3123 s	-	NH_3 asym. stretch

3056	457.27	129.29	-	3098 m	NH_3 sym. stretch
2974	11.71	31.38	2955 s	2963 vs	CH_2asym. stretch, C_4-H_{10} stretch
2971	26.6	68.29	-	-	C_{22}-H_{23} stretch
2963	2.19	68.6	-	2931 s	C_4-H_{10} stretch, CH_2asym. stretch
2917	9.13	73.71	-	2863 w	CH_2 sym. stretch
2876	26.67	51.24	-	-	C_{26}-H_{27} stretch
1836	404.17	7.78	1684 s	1696 w	C_{30}=O_{31} stretch
1734	392	7.66	--	-	C_2=O_7 stretch, NH_2 sci, NH_3 asym. bend, CH_2 sci
1692	188.47	2.15	1643 s	1642 s	COO^-asym stretch, NH_3asym. bend
1663	206.1	2.38	-	-	NH_3asym. bend, NH_2 sci
1634	95.51	4	1581 s	1591 m	NH_2sci
1615	126.37	8.65	1529 s	-	NH_3asym. bend
1517	85.98	7.76	-	1518 w	NH_3 sym. bend
1466	10.88	6.5	-	-	CH_2sci
1451	117.27	0.79	1428 vs	1424 vs	NH_3 asym. bend,CCstretch,C-OH bend,OH bend
1435	194.92	1.73	1399 sh	1402 m	COO^-symstretch,CCstretch,OHbend,CCH bend
1427	250.28	5.95	-	-	CO stretch, OH bend, NH_3 sym bend, CH bend, CH_2 sym bend
1386	104.24	0.64	1360 m	1356 s	O_{24}-H_{25} bend,C_{22}-H_{23} bend,C_{26}-H_{27} bend,O_{28}-H_{29} bend
1378	321.11	6.32	-	-	0_{28}-H_{29} bend,O_{32}-H_{33} bend,C_{26}-H_{27} bend,O_{24}-H_{25} bend,C_{22}-H_{23} bend,C-COO torsion,H_{10}-C_4 bend
1376	12.25	2.6	1360 m	-	OH bend,CH_2 bend,NH_3sym bend,
1367	158.84	9.79	1340 sh	-	CH_2 sci, CH bend
1332	13.03	4.14	1305 s	-	NH_3 sym bend,C_4-H_{10} bend,CH_2wag,NH bend, CN stretch
1319	23.85	0.67	-	1299 m	H_{27}-C_{26} bend,O_{32}-H_{33}bend,COO^-sym bend,O_{24}-H_{25} bend
1291	30.85	3.8	1262 m	-	H_{33}-O_{32} bend,C_{26}-H_{27} bend,C_{22}-H_{23} bend,O_{24}-H_{25}bend
1265	17.8	5.89	-	-	H_{33}-O_{32} bend,C_{26}-H_{27} bend,C_{22}-H_{23} bend, O_{24}-H_{25}bend,O_{28}-H_{29} bend
1252	17.44	5.62	1234 w	1233 s	CH_2 wag,CHbend,OH bend,NH_2 rock
1221	17.8	2.54	-	-	CH_2 twist,NH_3aym bend,NH_2rock,OH bend
1215	9.46	6.52	1214 m	-	O_{24}-H_{25} bend,C_{22}-H_{23} bend,C_{26}-H_{27} bend
1184	20.26	2.76	-	1187 vw	O_{13}-H_{14} bend,C_4-H_{10} bend,C_3-H_8 bend,NH_3 sym bend, NH_2 rock
1180	137.49	2.8	-	-	O_{32}-H_{33} bend,C_{26}-H_{27} bend,C_{22}-H_{23} bend, C_{26}-O_{28} strech, C_{30}-O_{32} strech
1160	23.66	3.44	1134 s	1140 m	NH_2 rock,NH_3 asymbend,OHbend,CH

					bend,CH_2 twist
1135	86.15	3.58	-	-	NH_2 rock,NH_3 asymbend,CH bend,CH_2 rock
1123	264.03	2.69	1102 sh	1100 s	O_{32}-H_{33} bend,O_{24}-H_{25} bend,C_{22}-H_{23} bend
1085	161.97	3.87	1074 s	1066 w	NH_3 rock
1071	15.45	2.85	-	-	NH_2rock,NH_3asym bend,CH_2 wag,CH bend
1045	199.75	9.56	-	1000 w	NH_2 rock,NH_3 asym bend,CH_2twist,OH bend,
996	170.39	2.99	-	-	NH_2 rock,NH_3 asym bend,CH_2 twist,OH bend
960	25.66	7.54	903 w	911 s	CH_2 rock,NH_2 rock,NH_3asym bend,C_{26}-H_{27}bend, C_{22}-H_{23} bend,O_{32}-H_{33} bend,O_{24}-H_{25} bend
959	23.79	6.16	-	-	CH_2 twist,NH_3 asym bend,NH_2 rock,C_4-H_{10} bend, C_{22}-H_{23} bend,O_{28}-H_{29} bend
890	2.41	1.25	875 sh	881 w	COO-sci,OH bend,C_{30}-C_{26} bend
882	0.72	4.98	841 w	842 vs	NH_3asym bend,CH_2wag,CO bend,CC bend
878	33.72	4.76	-	-	COO- sci,O_{33}-H_{32} bend,C_{27}-H_{26} bend,C_{22}-C_{20}bend, C_{25}-C_{26} bend
854	2.78	3.78	800 w	-	CH_2 rock,NH_3 asym bend,C_4-H_{10} bend,C_3-H_9 bend
831	5.74	1.79	790 m	795 s	COO- sci,O_{32}-H_{33} bend,C_{36}-H_{27}bend,C-C bend, O_{28}-H_{29} bend,NH_2 wag
820	35.97	3.32	-	-	NH_3 asym bend ,NH_2 twist ,CH_2 rock,0_{13}-H_{14} bend,C=O bend,CHbend,C-C bend
746	40.62	1.23	677 vvs	-	CH_2 rock,COO-sci,O_{32}-H_{33} bend,NH_2 wag, O_{28}-H_{29} bend
732	55.43	10.63	-	-	COO-sci,NH_3sym bend,NH_2 twist,O_{13}-H_{14} bend, CH_2 rock
725	101.21	2	-	662 w	COO-twist,NH_2 twist,CH_2 rock,NH bend
685	11.01	2.52	-	-	NH_3sym bend,CH_2 rock,COO-twist ,NH_2 rock
634	217.39	2.55	613 m	604 w	NH_2 twist,O_{28}-H_{29} bend,O_{24}-H_{25} bend,O_{32}-H_{33} bend
627	148.99	7.67	-	-	NH_2 wag,O_{24}-H_{25} bend,O_{32}-H_{33} bend, CH_2 rock,O_{28}-H_{29} bend
609	116.53	1.6	559 w	568 w	COO- sci,NH_2 wag,O_{32}-H_{33} bend,O_{28}-H_{29} bend
554	67.14	2.67	-	-	O_{28}-H_{29} bend,O_{24}-H_{25} bend,O_{32}-H_{33} bend,NH_2 wag
552	31.84	1.91	521 vw	519 m	CH_2 rock,NH_2 wag,COO-sci,O_{24}-H_{25} bend, O_{28}-H_{29} bend
542	30.03	1.67	-	-	CH_2 rock,O_{28}-H_{29} bend,NH_2 rock,O_{24}-H_{25} bend
510	70.3	3.45	502 vw	499 sh	O_{32}-H_{33} bend,O_{24}-H_{25} bend
491	114.4	0.85	-	-	NH_2 twist,CH_2 rock
481	35.28	3.55	480 vw	-	NH_2 rock,CH_2 rock,C_{26}-H_{27} bend, O_{32}-H_{33}bend,COO- sci,C_{22}-H_{23} bend

458	57	1.29	-	-	NH_2 rock,NH_3sym bending, O_{13}-H_{14} bend, CH_2rock,COO^-sci
439	25.72	0.36	-	392 w	O_{32}-H_{33} bend,O_{24}-H_{25} bend,O_{28}-H_{29} bend,NH_2 rock
433	30.63	0.41	-	-	NH_2 rock,CH_2 rock, O_{13}-H_{14} bend, NH_3sym bend
392	115.04	1.13	-	336 s	NH_2 wag,O_{28}-H_{29} bend,O_{24}-H_{25} out-of-plane bend
380	19.4	1.1	-	-	NH_3 sym bend,NH_2 twist,O_{24}-H_{25} bend,O_{28}-H_{29} out-of-plane bend,CH_2 twist,O_{13}-H_{14} bend
344	5.64	0.4	-	-	NH_3 torsion,O_{13}-H_{14} out-of-plane bend
330	9.11	1.4	-	-	NH_3 torsion,O_{32}-H_{33} out-of-plane bend
314	61.97	1.12	-	-	O_{13}-H_{14} out-of-plane bend,COO^- rock,NH_3 rock, C_4-H_{10} bend
303	77.89	1.08	-	297 w	NH_3 torsion,O_{13}-H_{14}bend,COO^- rock, C_3-H_8 bend, O_{28}-H_{29} bend, O_{24}-H_{25} bend
263	97.12	3.89	-	232 w	O_{13}-H_{14} out-of-plane bend
255	4.4	0.46	-	-	C-OOH torsion,C-OH torsion,O_{24}-H_{25} bend, O_{28}-H_{29}bend,O_{32}-H_{33} bend,O_{13}-H_{14} bend
210	4.43	0.13	-	189 m	NH_3torsion,COO^- wag,NH_2 rock,O_{24}-H_{25} bend, O_{28}-H_{29} bend
205	2.19	1.71	-	-	COO^- wag, NH_2 twist
179	32.01	0.94	-	164 sh	NH_2 twist,COO- wag, C_4-H_{10} bend,O_{24}-H_{25} bend
156	4.03	0.5	-	130 vvs	NH_3 sym bend,CH_2 wag, O_{32}-H_{33} bend, O_{13}-H_{14} bend
143	8.43	0.45	-	113 s	NH_3sym bend,CH_2 twist,C_4-H_{10} bend,O_{32}-H_{33} bend,
103	10.09	0.57	-	82 s	NH_2 rock,CH_2 rock, O_{13}-H_{14} bend
89	4.99	0.17	-	-	CH_2 rock,NH_2 wag,O_{32}-H_{33} bend, NH_3 sym bend,C_{11}-O_{12}bend,COO^- twist
85	4.87	0.31	-	-	NH_2 wag,O_{24}-H_{25} bend,COO^-twist,C_2-O_7 bend, O_{32}-H_{33} bend.
76	3.39	0.59	-	-	NH_2 wag,CH_2 rock, COO^-twist ,C_4-H_{10} bend, C-OH torsion,NH_3 torsion
70	0.54	0.28	-	-	C-OOH torsion,COO^-rock
59	8.25	0.4	-	-	C-OOH torsion,O_{28}-H_{29} bend, COO^- twist,NH_3 sym bend,NH_2 wag,C_4-H_{10} bend,O_{24}-H_{25} bend
52	3.18	0.22	-	--	COO^- twist, C-OH torsion,C-OOH torsion, NH_3sym bend,C_4-H_{10} bend
41	2.07	1.26	-	-	COO^-twist,CO bend,O_{28}-H_{29} bend,NH_2 wag, CH_2 wag

38	0.93	0.4	-	-	COO^- wag,C_{22}-H_{23} bend,NH_3 sym bend, NH_2 wag
27	0.88	0.02	-	-	C-OOH torsion, NH_3 rock, NH_2 wag.
12	2.75	0.25	-	-	NH_3 rock, COO^- wag,NH_2 twist,CH_2 wag, O_{24}-H_{25} bend,O_{13}-H_{14} bend

Carbonyl group vibrations

The carbonyl group stretching vibrations give rise to the characteristic bands in IR and Raman. The intensity of these bands can increase because of the formation of hydrogen bonds. The carbonyl group vibration is observed in the region 1760-1730 cm^{-1} (Silverstein & Webster, 2003; Smith, 1999). The strong band at 1684 cm^{-1} in IR and a weak band at 1696 cm^{-1} in Raman are assigned tocarbonyl stretching mode. The redshifting of carbonyl stretching mode is attributed to the fact that the carbonyl group chelate with the other nucleophilic group, thereby forming both intra- and intermolecular hydrogen bonding in the crystal Vidya *et al*., 2011).

Carboxylate group vibrations

The carboxylate ion gives rise to two modes, asymmetric and symmetric stretching, asymmetric stretching near 1650-1550 cm^{-1} and symmetric stretching near 1400 cm^{-1}(Bellamy, 1975). The asymmetric stretching mode of COO^- vibration appears in IR at 1643 cm^{-1} which is very strong and also a strong band is observed in Raman at 1642 cm^{-1}. The symmetric stretching COO^- vibration is identified in IR at 1399 cm^{-1} and in Raman at 1402 cm^{-1}. The lowering of COO^- stretching wavenumbers indicates the formation of hydrogen bonding. The COO- scissoring mode appears as a strong band at 677 cm^{-1} in IR. The wagging, rocking and scissoring modes of carboxylate vibrations have been identified and assigned (Table 2).

Hydroxyl vibrations

The hydroxyl stretching vibrations are generally observed around 3500 cm^{-1} (Silverstein & Webster, 2003). The broad band observed in IR at 3439 cm^{-1} corresponds to the O-H stretching vibration. The redshifting of O-H stretching wavenumber confirms the intra- and intermolecular O-H···O hydrogen bonding in the molecule. The inplane bending mode of O-H group usually appears as strong bands in the region 1440-1260 cm^{-1}. The medium IR band at 1360 and Raman band at 1356 cm^{-1} are assigned to inplane bending of the hydroxyl group which is coupled with C-H inplane bending mode. The weak band observed at 232 cm^{-1} in Raman is attributed to the O-H out of plane bending mode.

Methylene and methine group vibrations

The asymmetric and symmetric methylene stretching vibrations normally occur at 2926 and 2853 cm^{-1}. The CH_2 asymmetric stretching mode is observed as strong bands at 2955 and 2963 cm^{-1} in IR and Raman respectively. The weak band in Raman at 2863 cm^{-1} is assigned to CH_2 symmetric stretching mode which is coupled with CH stretching mode. The CH_2 scissoring mode coupled with bending of CH group contributes a band at 1340 cm^{-1} in IR. Various other bending, wagging and torsional modes of the CCC chain have also been observed.

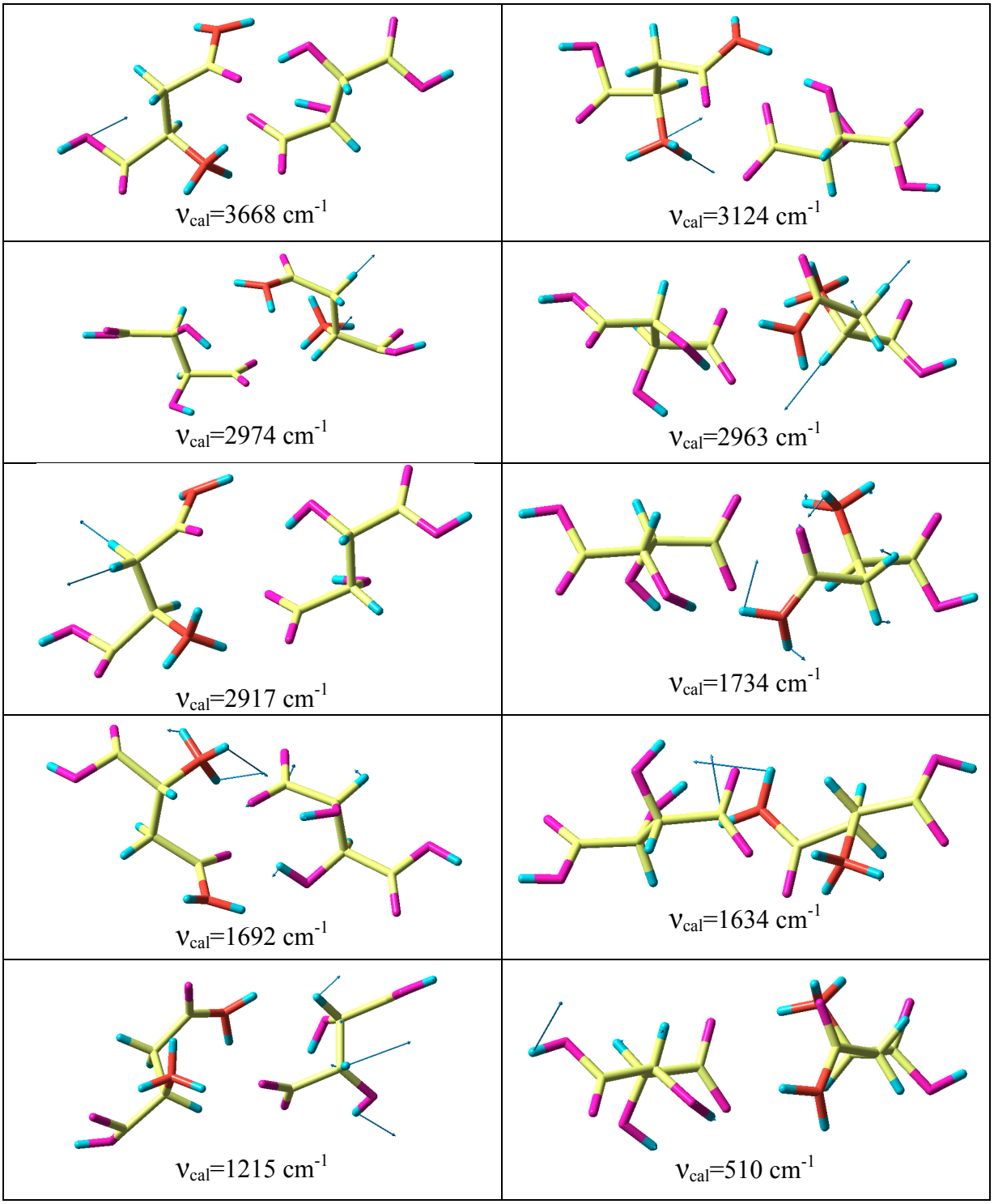

Fig. 4. Selected vibrational normal modes of LAT computed at B3LYP/6-31G* level

HOMO–LUMO gap

The energies of the highest occupied molecular orbital (HOMO) and the lowest unoccupied molecular orbital (LUMO) are computed at B3LYP/6-31G* level. HOMO and LUMO orbitals are shown in Fig. 5. Generally, the

energy values of LUMO, HOMO and their energy gap reflect the chemical activity of the molecule. HOMO as an electron donor represents the ability to donate an electron, while LUMO as an electron acceptor represents the ability to receive an electron. The smaller the LUMO and HOMO energy gaps, the easier it is for the HOMO electrons to be excited. In LAT, the HOMO is located on the tartrate moiety and the LUMO is only spre

This indicates charge transfer from tartrate to asparaginium moiety through the hydrogen bond, which is an important requirement to obtain large second order NLO responses. The energies of the HOMO and LUMO based on the optimized structure are computed at -0.23 and 0.28 eV, respectively. The HOMO-LUMO energy gap is 0.05 eV. The calculated HOMO and LUMO energies clearly show that charge transfer occurs within the molecule.

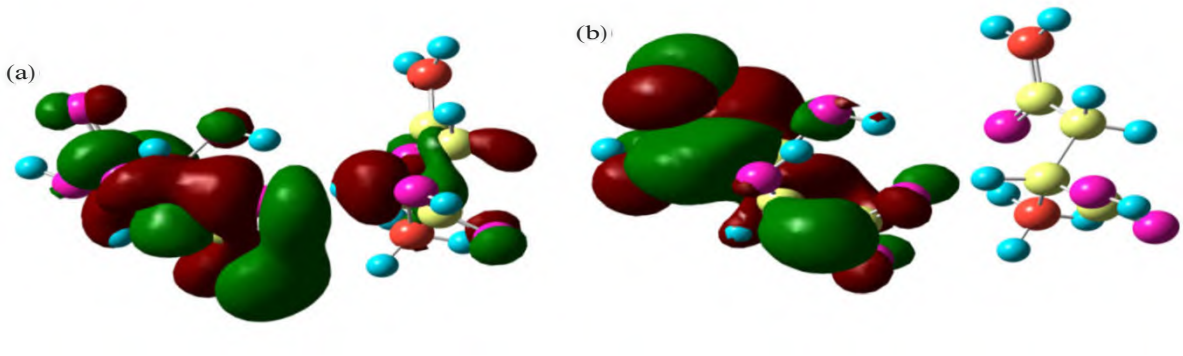

Fig. 5. (a) HOMO plot of LAT at B3LYP/6-31G* **(b)** LUMO plot of LAT at B3LYP/6-31G*

Conclusions

The single crystals of L- Asparaginium tartrate were grown by slow evaporation technique. The vibrational spectral analysis has been carried out based on B3LYP/ 6-31G* theory calculation. The optimized geometry shows, the carbon skeleton of the tartrate molecule is non-planar, with a C_{20}-C_{22}-C_{26}-C_{30} torsion angle. The difference in bond length between C=O of the tartarate moiety is due to different environment of oxygen. The redshifting of O-H stretching wavenumber confirms the intra- and intermolecular O-H···O hydrogen bonding. The lowering of HOMO and LUMO energy gap clearly explains the charge transfer interactions taking place within the molecule, which supports the NLO activity of the molecule.

References

Bellamy, L.J. (1975). *The Infra-red Spectra of Complex Molecules*. John Wiley and Sons, Inc., New York.

Casado, J. Ramirez F.J. and Navarrete J.T. (1995). Vibrational spectra and assignments of amino acid L-asparagine**.** *J. Mol. Struct.* **349:** 57–60.

Chemla, D.S. Zyss J. (Eds.) (1987). *Nonlinear Optical Properties of Organic Molecules and Crystals*, vols. 1(2) Academic Press, New York,

Colthup, N.B., Daly L.H. and Wiberley S.E. (1990). I*ntroduction to Infrared and Raman Spectroscopy*, Academic Press, New York.

Datta, A. and Pati, S.K. (2003). Dipole orientation effects on nonlinear optical properties of organic molecular aggregates. *J. Chem. Phys.* **118(18):** 8420-8427.

De Matos, G., Venkataraman, V., Nogueria, E., Belsley, M. Criado, P.A. Dianez, M.J. and Perez, G. (2000). Synthesis, crystal growthand characterisation of a new nonlinear optical material — urea l-malic acid, E. *Synth. Met*. **115:** 225-227.

Discoll, C.A., Hoffmann, H.J. Stone, R.E. and Perkins, P.E. (1986). Structural, vibrational and thermal studies of a new nonlinear optical material: l-Asparagine-l-tartaric acid. *J. Opt. Soc. Am.* **31:** 683–686.

Frisch, M.J., Trucks, G.W., Schlegel, H.B., Scuseria, G.E., Robb, M.A., Cheesemann, J.R., Scalmani, G., Barone, V., Mennucci, B., Petersson, G.A., Nakatsuji, H., Caricato, M., Hratchian, H.P., Izmaylov, A.F., Bloino, J.G., Zheng, J.L. Sonnenberg, M., Hada, M., Ehara, K., Toyota, R., Fukuda, J., Hasegawa, M., Ishida, T., Nakajima, Y., Honda, O., Kitao, H., Nakai T., Vreven J.A., Montgomery J., Peralta, J.E. Ogliaro, F.M., Bearpark, J.J., Heyd, E., Brothers, K.N., Kudin, V.N., Staroverov, R., Kobayashi, J., Normand, K., Raghavachari, A., Rendell, J.C., Burant, S.S., Iyengar, J., Tomasi, M., Cossi, N., Rega, J.M., Millam, M., Klene, J.E., Knox, J.B., Cross, V., Bakken, C., Adamo, J., Jaramillo, R., Gomperts, R.E., Stratmann, O., Yazyev, A.J., Austin, R., Cammi, C., Pomelli, J.W., Ochterski, R.L., Martin, K., Morokuma, V.G., Zakrzewski, G.A., Voth, P., Salvador, J.J., Dannenberg, S., Dapprich, A.D., Daniels, O., Farkas, J.B., Foresman, J.V., Ortiz, J. and Cioslowski, D.J. (2009). *Gaussian 09, Revision A.02, Gaussian, Inc.,* Wallingford CT.

Hierle, R.J. and Badamn, J.Z. (1984). Growth and characterization of a new material for nonlinear optics: Methyl-3-nitro-4-pyridine-1-oxide (POM), *J. Cryst. Growth* **69:** 545–554.

Kong, L., Yan, Q., Ji-Dong, Z., Xiu-Ping, J., (2008). Characterization of material for nonlinear optics. *ActaCryst.* **64:** 24-28.

Mallik, T., Kar, T., Bocelli, G., Musatti, A. (2006). Structural and thermal characterization of L-arginine dihydrate-a nonlinear optical material. *Cryst.Res. Technol.* **41:** 280–284.

Natarajan, S., Hema, V., Sundar, J.K. Suresh, J. and Lakshman, P.N. (2010). L-Asparagine-L-tartaric acid, *ActaCryst.* **66:** 22-39.

Pecaut, J. and Bagieu, B. (1993). 2-Amino-5-nitropyridiniummonohydrogenphosphite M. *ActaCrystallogr.* **49:** 834-838.

Ravikumar, C.I. and Hubert, J. (2010). Electronic absorption and vibrational spectra and nonlinear optical properties of 4-methoxy-2-nitroaniline. *Phys. Chem. Phys.* **12:** 94-98.

Ravikumar, C.I., Hubert, J. and Sajan, D. (2010). Vibrational contributions to the second-order nonlinear optical properties of π-conjugated structure acetoacetanilide. *Chem. Phys.* **36:** 9-1.

Ravikumar, C.I., Hubert, J. andJayakumar, V.S. (2008). Charge transfer interactions and nonlinear optical properties of push–pull chromophorebenzaldehydephenyl-hydrazone: A vibrational approach. *Chem. Phys. Lett*. **46:** 55-58.

Scott, A.P. and Radom, L. (1996). Harmonic Vibrational Frequencies: An Evaluation of Hartree−Fock, Møller−Plesset, Quadratic Configuration Interaction, Density Functional Theory, and SemiempiricalScale Factors**.** *J. Phys. Chem*. **100:** 16-23.

Shakir, M.B., Riscob, K.K., Maurya, V. Ganesh, M.A., Wahab, G. Bhagavannarayana, T. (2010). Unidirectional growth of l-asparagine monohydrate single crystal: First time observation of NLO nature and other studies of crystalline perfection, optical, mechanical and dielectric properties, *J. Cryst. Growth.* **312:** 3171–3177.

Silverstein, R.M. and Webster, F. (2003). *Spectrometricidetification of organic compounds,*Jonh Wiley and sons, New York.

Smith, B.C. (1999). *Infrared Spectral Interpretation, A Systematic Approach*, CRC Press, Washington.

Srinivasan, P.T., Kanagasekaran, R., Gopalakrishnan, G., Bhagavannarayana, P. andRamasamy, R. (2006). Studies on the Growth and Characterization of l-AsparaginiumPicrate (LASP) A Novel Nonlinear Optical Crystal, *Cryst. Growth Des.* **6:**1663–1670.

Vein, D.L., Colthup, N.B., Fateley, W.G. and Grasselli J.G. (1991).ss*The Handbook of Infrared and Raman Characteristic Frequencies of Organic Molecules*, Academic Press: New York.

Vidya, S.C., Ravikumar, I., Hubert, J.P., Kumaradhas, B., Devipriya, D. and Raju, K. (2011). Vibrational spectra and structural studies of nonlinear optical crystal ammonium D, L-tartrate: a density functional theoretical approach, *J. Raman Spectrosc.* **42:** 676-678.